

Glider Salinity Correction for Unpumped CTD Sensors across a Sharp Thermocline

17

Yonggang Liu*, Robert H. Weisberg, Chad Lembke

College of Marine Science, University of South Florida, St. Petersburg, FL, USA

*Corresponding author: E-mail: yliu18@gmail.com, yliu@mail.usf.edu

CHAPTER OUTLINE

1. Introduction	305
2. A Sharp Thermocline	307
3. Methods	310
4. Thermal Lag Correction Results.....	313
4.1 Successes and Limitations	313
4.2 Improvements with a Median Filter	314
4.3 Average of Upcast and Downcast Profiles	318
5. Summary and Discussions	320
Acknowledgments	321
References	321

1. INTRODUCTION

By offering economical platforms for interdisciplinary ocean observations, autonomous underwater gliders (hereafter “gliders”) are becoming important assets of ocean observing systems.^{1–3} Gliders are robots that propel themselves through the water using changes in buoyancy and adjustments in attitude to allow them to soar on wings. By cyclically falling and floating, they progress forward in a sawtooth fashion while transiting from near the surface to the seafloor or desired depth. Those powered on batteries are capable of being deployed weeks to months, allowing 100–1000s of km transects of water column data to be collected. Several commercial products are available, for example, the Slocum glider created by and offered commercially by Teledyne Webb Research Corporation,^{4,5} the Seaglider developed at the Applied Physics Laboratory at the University of Washington and now available through Kongsberg Maritime,⁶ and the Spray glider of Scripps Institution of Oceanography and Bluefin Robotics.⁷ Their applications are found in many regions

of the world's oceans, e.g., the US West Coast,^{8,9} the US East Coast,^{10,11} the Gulf of Mexico,^{3,12–16} the Mediterranean Sea,¹⁷ and the Australia coast.^{18–20}

For salinity determinations, some of the gliders use passive (unpumped) conductivity cells to conserve power and extend the range of the glider mission. As with conventional CTDs, there is a mismatch between the temperature and the conductivity measurements primarily due to the thermal inertia of the conductivity sensor. It takes time for the conductivity sensor to adjust to surrounding water, e.g., to diffuse its heat stored when it moves from hot to cold water, whereas the temperature sensor responds more rapidly to the ambient temperature change. This temperature–conductivity response time mismatch leads to erroneous salinity calculations, referred to as thermal lag effects. Such effects were examined by Gregg and Hess²¹ and Lueck,²² and a numerical algorithm for thermal lag correction was proposed by Lueck and Picklo.²³ A practical method for determining the thermal lag correction parameters was proposed by Morison et al.²⁴ based on minimizing the salinity separation of temperature–salinity (T – S) curves from the upcasts and downcasts of a yo-yo sequence of conductivity–temperature–depth (CTD) profiles. The thermal lag corrections for two Sea-Bird CTD instruments (SBE-41CP and SBE-41) were reported by Johnson et al.²⁵ based on screening thousands of profiles from Argo profiling floats. Mensah et al.²⁶ revisited the thermal mass inertia correction of SBE4 conductivity sensors for the calculation of salinity, and they proposed an empirical method, also based on Morison et al.²⁴ to determine optimal values for the correction parameters.

Unlike conventional CTD casts from a surface vessel where the ascent/descent speeds may be controlled to be constant and slow enough, a glider's speed may vary through the water depending on the glider's buoyancy manipulation, altitude, and depth. The glider moves both horizontally and vertically. A complete descent and ascent course of the glider is called a yo-yo. The conductivity measurement relies on the glider's motion through the water to passively flush the conductivity cell. The rate of flushing is related with glider altitude and speed, and varies during the course of a yo-yo. Also, the glider's CTD sampling frequency is often set to be lower (~ 0.5 Hz) than that of the high-resolution sampling of the CTD operated on a surface vessel, and the sampling interval may be irregular. In particular, some glider data acquisition systems do not sample the CTD sensors at a constant rate, nor do they collect data continuously, depending on how the glider firmware was programmed on a mission and how many sensors it has reporting to it in a given sequence. The glider data output may not be a continuous and evenly spaced time series, even though the glider is set up to sample at a constant rate. There can be gaps that are substantial. The users have no way of knowing the exact time stamp placed on the data (personal communication, Carol Janzen, Seabird Scientific). These features render glider CTD data different from traditional CTD data, and the thermal lag correction is more difficult. This issue is discussed in recent publications.^{27–29}

For salinity data from unpumped CTD sensors installed on gliders, proper corrections are critical prior to their applications in physical oceanography,

e.g., hydrographic analysis,^{30,31} mixed layer depth estimation,³² assimilation into ocean circulation models,^{33–35} multiplatform analysis,³⁶ etc. Salinity data also affect the calculation of other variables and derivatives, e.g., dissolved oxygen, chlorophyll, and spiciness.^{8,37–39} Careful calibration of salinity data is, therefore, of primary importance in glider data processing.

Thermal lag corrections for glider data have gained increased attention in recent years. For example, Bishop²⁷ corrected the thermal lag effects in Slocum glider observations⁵ based on the methods of Lueck and Picklo²³ and Morison et al.²⁴ He used the mean vertical speed of the Slocum glider to calculate the correction parameters. Eriksen⁴⁰ reported salinity estimation using an unpumped conductivity cell on a Seaglider. Frajka-Williams et al.²⁸ briefly described the thermal inertia corrections of Seaglider data based on the flight model of Eriksen et al.⁶ and the thermal lag theory of Lueck.²² Their relaxation constants were determined by minimizing the along-isopycnal difference between salinities of successive climb–dive near the surface or dive–climb at depth. Recently, Garau et al.²⁹ proposed a thermal lag correction method for Slocum CTD glider data, also based on the work of Morison et al.²⁴ but using the variable speed of the glider. Another novel part of that method is that the four correction parameters are determined by minimizing an objective function that measures the area between two T – S curves formed by two CTD profiles, one upcast and one downcast. This method has been used in routine glider data processing.^{41,42}

Thermal lag effects for glider data may vary with water column stratification. For a well-mixed water column, the thermal lag effects may not be a problem at all, because the water properties are about the same throughout the water column, and the time lags in temperature and conductivity sensors may not be noticeable. However, in a stratified water column, the thermal lag effects may become an issue.⁴³ The stronger the stratification, the larger the expected thermal lag effects.²⁶ The importance of correcting the thermal lag effects was demonstrated for the SBE-25 CTD data collected in the Mediterranean summer thermocline.⁴⁴

In this paper, we examine the performance of the thermal lag correction methods in correcting the salinity errors in the glider data collected on the eastern Gulf of Mexico, West Florida Shelf (WFS), with emphasis on a strong thermocline. The purpose is two-fold: (1) to test the existing thermal lag correction methods in the case of a strong thermocline, and (2) to improve the glider salinity correction results empirically.

2. A SHARP THERMOCLINE

Since 2009, Webb Slocum gliders (model G1 with a 200-m buoyancy engine) have been added to integrated ocean observation systems on the WFS⁴⁵ that include arrays of moored Acoustic Doppler Current Profilers,⁴⁶ high-frequency radars,^{47,48} and satellite-tracked drifters.⁴⁹ These glider data have been used in oceanographic applications and data assimilation experiments on the WFS.^{13–15} Unpumped glider

CTD assemblies of Seabird Electronics Inc. are used on Slocum gliders up through 2010. The sensors are electronically derived from the SBE41CP Argo float CTD. It is important to recognize that they are distinctly very different from the instrument/CTD as used on the Argo profiling floats. This means processing applied to SBE41CP Argo profiling float data (or any pumped CTD data set) cannot be directly transferred to the glider unpumped CTD data processing (personal communication, Carol Janzen).

As a low-energy shelf,^{47,50} the eastern Gulf of Mexico water tends to be stratified in spring and summer,⁵¹ which is related to the seasonal variations of the wind forcing and heating/cooling.^{52–55} Interactions between the Loop Current eddies and the shelf slope could ventilate the WFS with cold waters of deep ocean origin^{13,14,56} and generate a strong thermocline on the shelf.

A particular example can be seen from the glider data of mission 16 between the 25- and 50-m isobaths (Figure 1). Even though this glider mission was of short duration (aborted due to an air bladder leak after three days of survey in April of 2009), a sharp thermocline was observed in the area offshore of the 40-m isobath. Both the temperature and conductivity data show a distinct difference between the upper layer and the near bottom layer of the water column with a sharp thermocline around the 30-db level (Figure 2(a) and (b)). The calculated salinity data show a thin lens of saline water in the transect plot (Figure 2(c)), which corresponds to the vertical level of the thermocline. This feature cannot be interpreted as a slope water lens transported on-shelf within the thermocline as found by Hopkins et al. (2012) in the Celtic Sea⁵⁷;

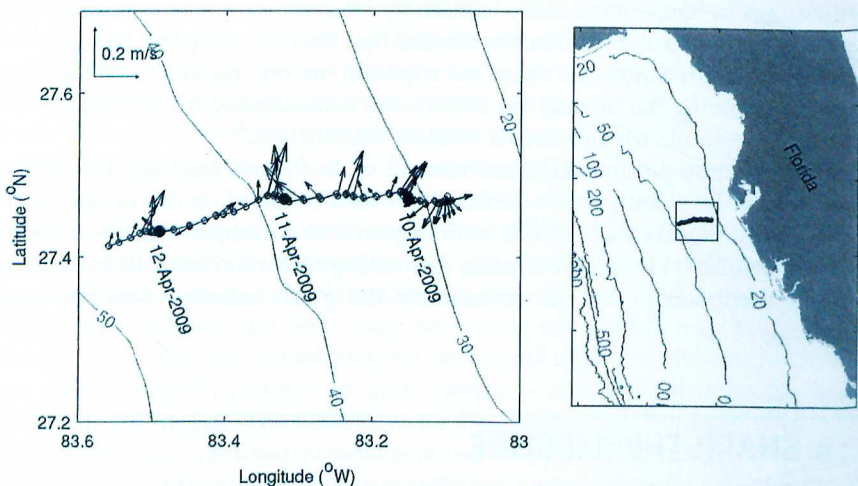
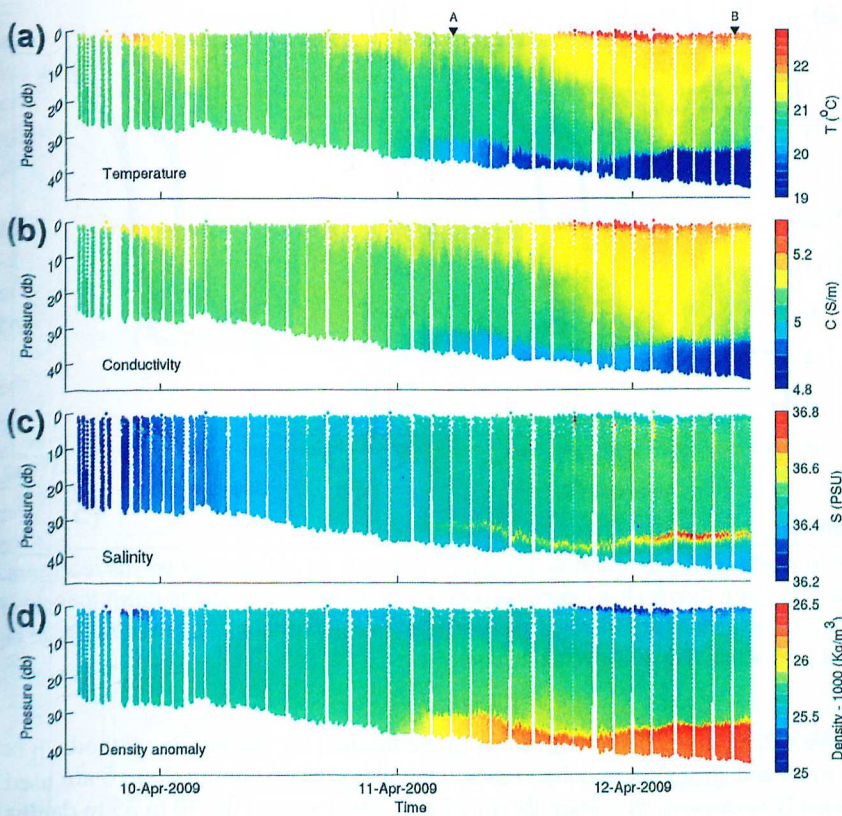


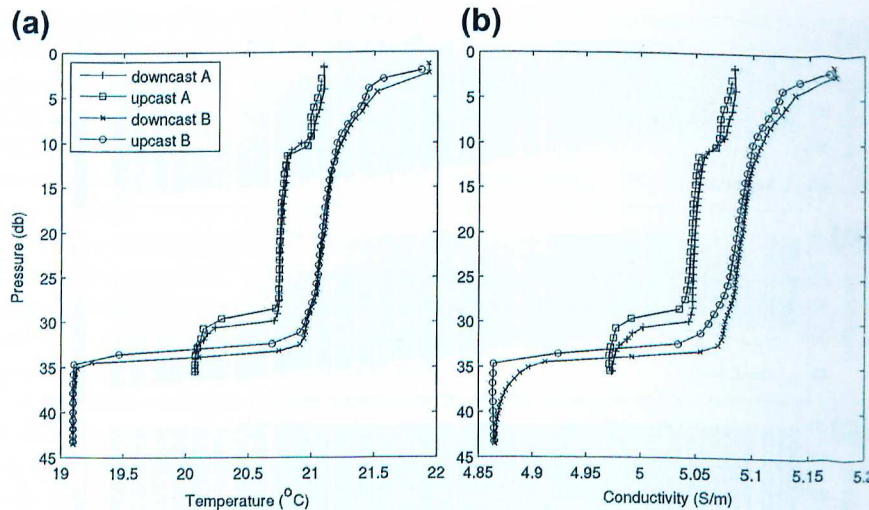
FIGURE 1

Glider track and the surface velocity estimated from the glider observations (left panel), and the relative position of the track on the West Florida Shelf (right panel). Bottom bathymetry contours are in meters.

**FIGURE 2**

Water property distributions along the Figure 1 glider transect: (a) temperature, (b) conductivity, (c) salinity, and (d) density anomaly. Note the false high salinity lens around the 30-m depth level (c) where the thermocline is located, and the associated vertical density inversion (d). The upside-down triangles in panel (a) denote the locations of two yo-yos in weak and sharp thermocline cases, respectively. The gaps between the profiles correspond to the time window for data transfer when the glider floated on the surface.

rather, it is due to persistent thermal lag errors on the glider salinity calculations in the presence of a strong thermocline. This can be evidenced as follows: (1) The density transect shows vertical inversions (heavier water on top of lighter water, Figure 2(d)) as a result of this salinity artifact; (2) The vertical profiles of temperature show mismatches around the thermocline between the downcast and upcast of a glider yo-yo (Figure 3(a)); (3) The vertical profiles of conductivity show even more obvious mismatches at those levels between the downcast and upcast of a glider yo-yo (Figure 3(b)); and (4) The ascending and descending vertical profiles of salinity exhibit errors of opposite sign near the thermocline (Figure 4). These are typical features related to the thermal lag effects of CTDs across a sharp thermocline.²⁶

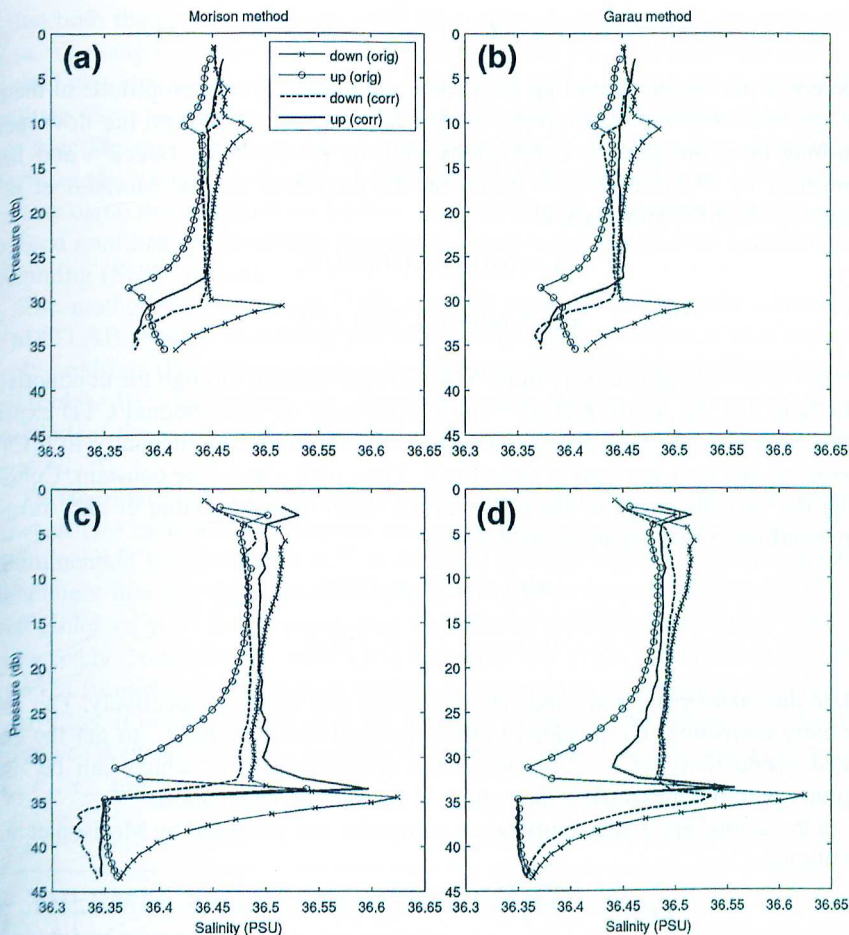
**FIGURE 3**

Vertical profiles of the temperature (a) and conductivity (b) of two glider yo-yos representing weak and sharp thermocline cases, respectively (denoted as the upside-down triangles in Figure 2). Note the sharp thermocline near ~ 34 m depth with a temperature change of about 2°C within 3 m of the water column.

We will examine the effectiveness of the thermal lag correction methods in both the weak and strong thermocline cases. The glider data from mission 16 are used in this study because of this sharp thermocline located around the 30 to 35 m depths of the water column. Temperature changes are about 2°C within 3 m of the water column at the 45-m site (Figure 3(a)). In terms of the vertical temperature gradient, this case may be referred to as a “strong thermocline” according to Mensah et al.²⁶ Along the transect, the strength of the thermocline decreases toward the land. Two yo-yos (points A and B in Figure 2(a)) are chosen to represent a weak and a strong thermocline, respectively. The horizontal distances the glider maneuvered during the two yo-yos are 60 and 84 km, respectively.

3. METHODS

As mentioned, a mismatch in the temporal response of a pair of temperature and conductivity sensors can lead to significant errors in the calculated salinity. So, the thermal lag correction methods, based on theoretical model of Lueck,²² are generally categorized into two approaches: to estimate the conductivity data measured inside the conductivity cell, or to estimate the temperature of water inside the conductivity cell, with the sole purpose of calculating salinity. This has been well documented in literature.^{24,26,29}

**FIGURE 4**

Vertical profiles of the original and corrected salinity of one glider yo-yo (denoted as the upside-down triangles in Figure 2) using different methods: (left panels) Morison et al. (1994) and (right panels) Garau et al. (2011). Thermal lag correction is successful for the weak thermocline profile (panels (a) and (b)), but not for the sharp thermocline case (panels (c) and (d)). Salinity spikes near the sharp thermocline are still seen in the corrected salinity profiles.

In the first approach, a conductivity correction (C_T) may be expressed as follows:

$$C_T(n) = -bC_T(n-1) + \gamma a[T(n) - T(n-1)], \quad (1)$$

where n is the sample index, T is the temperature, and γ is the sensitivity of conductivity to temperature. The coefficients a and b are given as follows:

$$a = \frac{4f_n\alpha\tau}{1 + 4f_n\tau}, \quad (2)$$

$$b = 1 - \frac{2a}{\alpha}, \quad (3)$$

where f_n is the Nyquist sampling frequency, and α and τ are the amplitude of the error and time constant, respectively. Both α and τ are dependent on the flow speed (flushing rate) through the conductivity cell, as predicted by Lueck²² and later confirmed by Morison et al.²⁴ Based on the empirical results, Morison et al.²⁴ suggested the following formulas:

$$\alpha = 0.0135 + 0.0264/V, \quad (4)$$

$$\tau = 7.1499 + 2.7858/\sqrt{V}, \quad (5)$$

where V is the average velocity (units in meters per second) through the conductivity cell. Note that the Morison et al.²⁴ study was based on conventional CTD experiments, in which the flow speed is known (may be controlled manually in a CTD operation) and then assumed to be constant. Thus, both α and τ are constant. Considering the variable speed of the glider in the water column, Garau et al.²⁹ further expressed these two equations as follows:

$$\alpha(n) = \alpha_o + \alpha_s/V(n), \quad (6)$$

$$\tau(n) = \tau_o + \tau_s/\sqrt{V(n)}. \quad (7)$$

where the subscripts o and s indicate the offsets and slopes, respectively. The conductivity correction, C_T , is added to the measured conductivity, C , to get the estimated conductivity, $(C_T + C)$, outside the conductivity cell, which can be used together with the measured temperature, T , for salinity calculation.

In the second approach, temperature correction was proposed by Morison et al.²⁴ as follows:

$$T_T(n) = -bT_T(n-1) + a[T(n) - T(n-1)], \quad (8)$$

where a and b are the same as those defined in Eqns (2) and (3). The temperature correction T_T is added to the measured temperature T to get the estimated temperature ($T_T + T$) inside the conductivity cell, which can be used together with the measured conductivity C for salinity calculation.

The conductivity correction was used by some researchers,^{23,26} whereas the temperature correction was preferred by others.^{24,29} Note that Eqn (8) is simpler than Eqn (1) because it does not need the estimated sensitivity γ . Also, it avoids the error induced by implicitly linearizing the equation of state in the first approach (by effectively assuming a uniform ratio between temperature and conductivity).

The process for choosing the parameters α_o , α_s , τ_o , and τ_s is critical in the thermal lag correction. Morison et al.²⁴ proposed a practical (empirical searching) method to determine these parameters by minimizing the salinity separation of $T-S$ curves from upcasts and downcasts of a yo-yo sequence of CTD profiles. The hypothesis

that both the upcast and downcast CTD profiles should measure the same water mass. The empirical results are given in Eqns (4) and (5). This empirical searching method was also used in Mensah et al.²⁶ Garau et al.²⁹ proposed another method to estimate these parameters based on the same hypothesis. They minimize an objective function that measures the area between two $T-S$ curves from upcasts and downcasts of a yo-yo sequence of CTD profiles. The minimization is an iterative process using the optimization toolbox from MATLAB. The minimum of the constrained nonlinear multivariable function is found using a sequential quadratic programming (SQP) method.

The method of Garau et al.²⁹ has received attention in the glider community. A MATLAB toolbox containing the thermal lag correction code is also available freely online (<http://www.socib.es/~glider/doco/gliderToolbox/ctdTools/thermalLagTools>). Its applications are found in many studies.^{41,58} However, to our knowledge, the correction for salinity data in a strong thermocline has not been reported.

The thermal lag correction code provided by Garau et al.²⁹ allows for a choice between two methods: (1) constant correction parameters for Eqns (6) and (7) as recommended by Morison et al.²⁴ in Eqns (4) and (5), and (2) variable correction parameters that are determined from a downcast-upcast pair of CTD profiles of each glider yo-yo.²⁹ In this paper, they are referred to Morison and Garau methods, respectively. Note that the velocity in Eqns (6) and (7) is not constant, which is different from that of the original method developed for conventional CTD casts.²⁴ Regardless, it is still referenced as the Morison method in this chapter. So, the only difference between these two methods is the choice of the four correction parameters α_o , α_s , τ_o , and τ_s .

4. THERMAL LAG CORRECTION RESULTS

4.1 SUCCESSES AND LIMITATIONS

The two correction methods mentioned previously were applied to the two CTD profiles shown in Figure 3, and the results of thermal lag correction are shown in Figure 4. Both the original and corrected salinity profiles are shown in the same panels so that the successes and limitations of the corrections may be seen.

For the weak thermocline, both methods successfully adjusted the salinity profiles (Figure 4(a) and (b)). The differences between the downcast and upcast salinity profiles are significantly reduced, especially for the two (weak) thermocline layers around the 12- and 30-m levels, respectively. The corrected downcast and upcast salinity profiles tend to align with each other throughout the water column. Two haloclines, one weaker around the 12-m level and the other stronger around the 30-m level, are evident in the corrected salinity profiles. These features correspond well with the weak thermoclines (Figure 3(a)) and the vertical gradients of conductivity at those two levels (Figure 3(b)), respectively. Despite the minor differences

(<0.02 PSU) between the upcast and downcast profiles, the thermal lag corrections for the weak thermoclines are satisfactory.

For the strong thermocline, the differences between the downcast and upcast salinity profiles are also reduced by both methods (Figure 4(c) and (d)). For example, the salinity spikes are reduced by 0.08 to 0.1 PSU using the Garau method (Figure 4(d)). However, salinity spikes are still seen in the corrected profiles near the strong thermocline around the 30- to 35-m levels. Note that both the temperature and conductivity profiles are reasonably smooth at these levels (Figure 3(a) and (b)). These salinity spikes are due to the short-term mismatch between the temperature and conductivity sensors.²⁶ The examples of salinity spikes, as shown in Figure 4(c) and (d), are not isolated cases. Persistent spikes are seen in the calculated salinity in this strong thermocline area. For some glider yo-yos, the salinity spikes of the downcast and upcast profiles point to different directions (i.e., one in $S +$ direction, the other in $S -$ direction) instead of one direction as shown in Figure 4(c) and (d). After the preliminary thermal lag correction using the Morison method, the salinity spikes in the downcast profiles are removed, whereas those in the upcast profiles are only slightly reduced (Figure 4(c)). However, using the Garau method, both salinity spikes are still present, though largely reduced compared with the original salinity data (Figure 4(d)). These preliminary experiments show that thermal lag effects are still a problem for the strong thermocline, and further improvements are needed for the thermal lag corrections.

It is worthy to point out that proper visualization is important in the examination of the salinity errors due to the thermal inertia effects. If shown in a transect plot as Figure 2(c), the preliminarily corrected salinity data are almost “acceptable” because the reduced salinity spikes are hardly seen from such a color plot (figure not shown). However, if shown in line plots (Figure 4(c) and (d)), these salinity errors are more evident. Another example is the very weak thermocline around the 12-m level at point A. It is not eye-catching at all in either the temperature or the conductivity profiles (Figure 3(a) and (b)). However, the original salinity data, directly calculated from these temperature and conductivity data, show a noticeable salinity difference (~ 0.07 PSU) between the upcast and downcast profiles (Figure 4(a) and (b)). Such salinity differences are not easily seen from the scattered color dots (Figure 2(c)) generated by the MATLAB internal function “scatter,” which is widely adopted by the glider community. These differences are usually too small to be resolved by the colors over a large range. These small features are not easily seen in color contour plots because the color contour plots are a smoothed version of the scattered dots. As a result, one should be cautious in interpreting the color scatter or contour plots of salinity for a halocline or for thermal lag effects. It is better to examine them in line plots as in Figure 4.

4.2 IMPROVEMENTS WITH A MEDIAN FILTER

Salinity spikes were seen from CTD profiles through sharp thermoclines/haloclines in early studies.⁵⁹ These salinity spikes were in error and cannot be eliminated by the

regular smoothing (e.g., low-pass filtering) technique that usually spreads the error and leaves its integral effect unchanged.²² Emery and Thomson⁶⁰ suggested some methods for detecting and removing large errors or spikes from data. A standard method for isolating large errors is to compute a histogram of the sample values, and see if the divergent values fit into the assumed probability distribution function for the assumed variable. Another method, which is more automatic and objective, is to identify and eliminate all values that exceed a specified standard deviation (e.g., three standard deviations). However, these approaches have the weakness that they must first consider all the data points, including the extreme values, as valid in order to determine which data points are outliers.⁶⁰ These conventional approaches are not effective or convenient for ridding glider data of salinity spikes. Mensah et al.²⁶ proposed a median filter to deal with these spikes in CTD profiles. Salinity profiles are slightly corrected by replacing, for a centered window of N points, the value at the center point by the median value of this window:

$$S(n) = \text{median}\left(S_{n-(N-1)/2}, \dots, S_{n-1}, S_n, S_{n+1}, \dots, S_{n+(N-1)/2}\right). \quad (9)$$

The one-dimensional median filter is a nonlinear digital filtering technique, often used to remove noise from a sequence of data. Using this technique for temperature, conductivity, and salinity, Mensah et al.²⁶ found that the spikes were effectively corrected so that errors spanning across a wide range of depth through the profile were identified.

To see the effect of de-spiking by this median filter, the salinity profile at point A is used as an example. Different filter window lengths (N) are used and the results are shown in Figure 5. The median filter is effective in removing the peaks from the profile data. A 5-point median filter ($N = 5$) can largely reduce the peaks of the spikes near the haloclines. When using 11 points or more, almost all the peaks are removed (actually replaced with the median values). To be conservative, a 7-point median filter ($N = 7$) is chosen for the following calculations. This corresponds to about 7 m in the vertical water column for this glider yo-yo (Figure 5). The depth range may vary as the speed of the glider changes.

The median filter is applied to the salinity data at point B (in Figure 2). A simple application of the median filter to the original salinity data can effectively remove the sharp spike in the upcast profile, and it can significantly reduce the large peak in the downcast profile. The median filter is further applied to the preliminarily corrected salinity profiles using the Morison method, and the spike in the corrected upcast profile is completely removed (Figure 6(a)). The improvement of the results is significant, which can be seen by comparing Figure 6(a) (filtered profiles) with Figure 4(c) (not filtered profiles).

Application of the median filter in conjunction with the Garau method is more complicated than with the Morison method. To obtain the optimal correction parameters, the temperature and salinity profiles are used to compute the area encompassed by the downcast and upcast profiles in the $T-S$ diagram (e.g., Figure 7), which is to be minimized in an iterative process. Thus, for each iteration, the median filter is

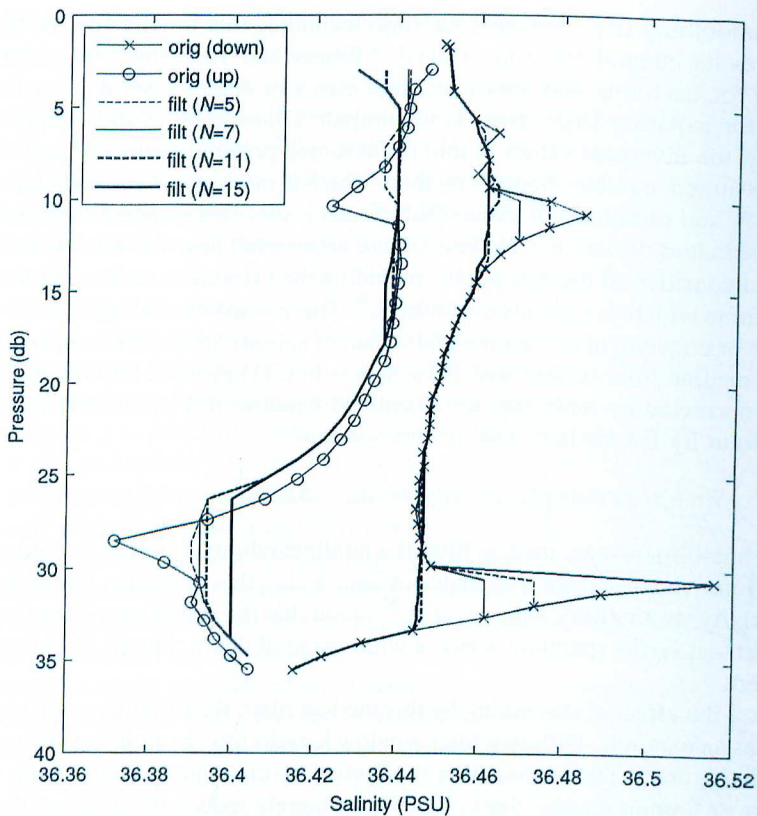


FIGURE 5

Vertical profiles of the salinity of one glider yo-yo (indicated as point A in Figure 2) before and after removing the salinity spikes using the median filter (N is the number of data points in a median filter window).

applied to the salinity data before they are used to calculate the $T-S$ area. After the correction, the median filter is applied to the salinity profile one more time to remove the spikes, if still present. The improved results are shown in Figure 6(b). The differences between the downcast and upcast salinity profiles are minimized, especially those spikes in the strong thermocline (with salinity errors of 0.13 PSU), which are effectively removed. Significant improvements are seen in the salinity correction.

The difference of the $T-S$ diagrams with and without the application of the median filter is evident. The area between the downcast and upcast profiles (using the corrected salinity) becomes smaller when the median filter is used (Figure 7). That is to say, the differences between the downcast and upcast water property (T and S) are reduced when the median filter is used in conjunction with the Garau method.

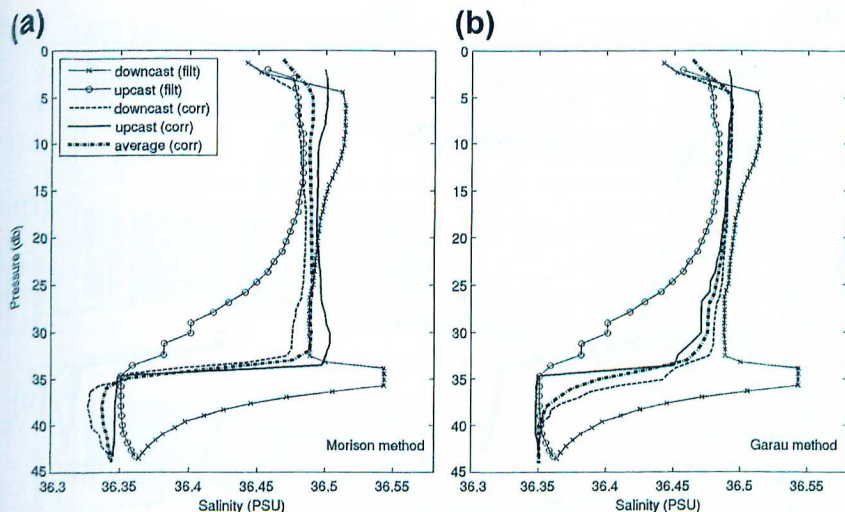


FIGURE 6

Vertical profiles of the de-spiked and the corrected salinity of one glider yo-yo (denoted as point B in Figure 2) using different methods: (a) Morison et al. (1994) and (b) Garau et al. (2011). An average of upcast and downcast salinity profiles is also shown.

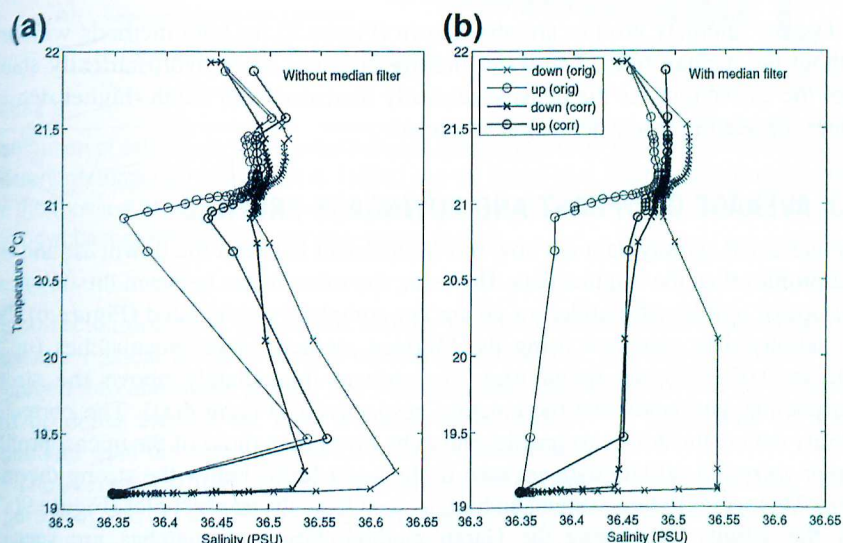
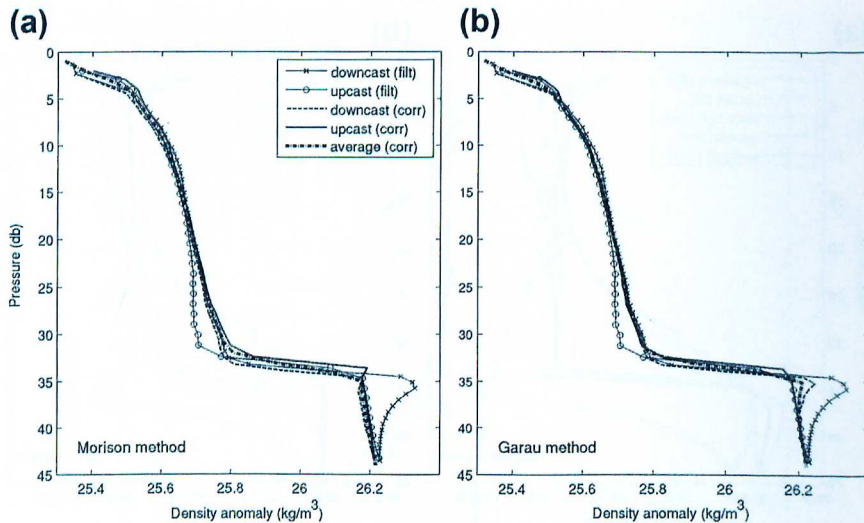


FIGURE 7

Temperature–salinity diagrams of the original and the thermal lag adjusted glider CTD data using Garau et al. (2011) method before (a) and after (b) removing the salinity spikes near the sharp thermocline using the median filter.

**FIGURE 8**

Vertical density anomaly (defined as density – 1000) profiles of one glider yo-yo (denoted as point B in Figure 2) after the salinity data are de-spiked and corrected using different methods: (a) Morison et al. (1994) and (b) Garau et al. (2011). An average of upcast and downcast density profiles is also shown for each case.

Density anomaly profiles are also shown (Figure 8) for both methods with and without the median filter. The water density becomes more hydrostatically stable after the corrections, as the density generally increases with depth (higher density values are seen in lower depths) as expected.

4.3 AVERAGE OF UPCAST AND DOWNCAST PROFILES

The corrected salinity data are now more consistent between the downcast and upcast profiles than the original data. However, the mismatches between the downcast and upcast profiles of a glider yo-yo are not completely eliminated (Figure 6). For the salinity data corrected using the Morison method, larger mismatches (up to 0.02 to 0.03 PSU) are found near the surface, immediately above the strong thermocline, and below the thermocline, respectively (Figure 6(a)). The corrected salinity data in the downcast profile tend to be lower than those of the upcast profile. Lower corrected salinity data are seen in the water levels below the strong thermocline. This seems to be a systematic bias, as seen from the transect plot (Figure 9(a)). For the salinity data using the Garau method, larger mismatches are seen in the strong thermocline (Figure 6(b)). These minor issues remain in the corrected salinity profiles.

A simple average between the downcast and upcast profiles seems to have a more acceptable salinity profile for the glider yo-yo (Figure 6). To facilitate the averaging,

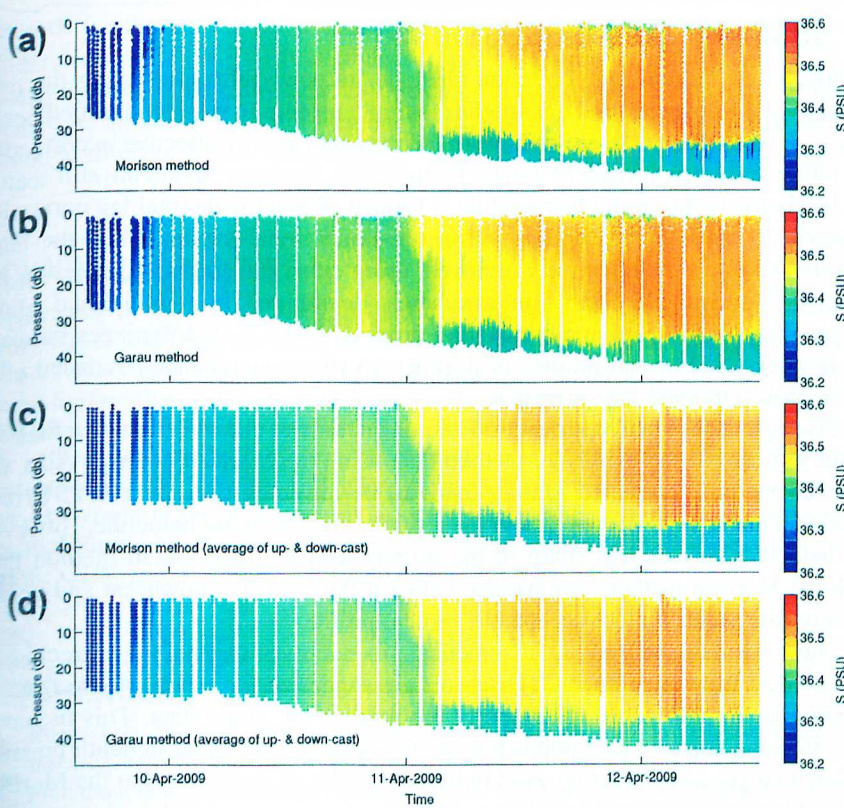


FIGURE 9

Distribution of salinity along the glider transect after correction of the thermal lag effect using different methods: (a) Morison et al. (1994) and (b) Garau et al. (2011). Salinity spikes near the thermocline depths are removed after applying the median filter. The averages of upcast and downcast salinity profiles are also shown (c & d).

The corrected downcast and upcast salinity profiles are first linearly interpolated to the same vertical levels at integer decibars, respectively. The two profiles are then averaged into one single profile. The averaged data, one profile for one yo-yo, would still be dense enough for most oceanographic studies.^{61,62} These data are more redundant than the conventional CTD casts from vessels.

The averaged salinity data are shown in Figure 6(a) and (b) as line profiles, and in Figure 9(c) and (d) as transect plots. The main differences between the two types of salinity correction are that the Morison method—corrected salinity data tend to be systematically lower by 0.01 PSU in the water levels below the strong thermocline, while the Garau method—corrected data are closer to the true data in the layer below the strong thermocline. However, using the Garau method, the halocline may be a bit smoothed in the salinity data corrected (Figure 6(b)).

5. SUMMARY AND DISCUSSIONS

Although new thermal lag correction methods are powerful for adjusting the mismatches of the downcast and upcast glider salinity profiles in weakly stratified ocean waters or weak thermoclines, we have found they are not very effective in correcting the salinity errors in the case of a sharp thermocline. Persistent spikes are still seen at the levels where the strong thermocline is located. When the thermal lag correction methods are used in conjunction with a one-dimensional median filter, the large salinity spikes can be effectively removed, using either the constant correction parameters²⁴ or variable correction parameters determined from individual glider yo-yos through an iterative minimization process.²⁹ The $T-S$ differences between the downcast and upcast profiles of a glider yo-yo are significantly reduced after the improved thermal lag correction.

The mismatches between the corrected downcast and upcast salinity profiles are slightly smaller using the Garau method than using the Morison method. Also, the Morison method—corrected salinity tends to be lower by 0.01 to 0.02 PSU than the Garau method—corrected data in the levels below the strong halocline. However, the halocline may be less sharp in the salinity data with the Garau method than with the Morison method. An average between the corrected downcast and upcast salinity data yields a more acceptable vertical profile.

Thus, based on the studies,^{24,29} practical procedures of thermal lag correction of salinity data from unpumped CTD sensors are suggested for waters of strong stratification as the following: (1) Properly pre-process the glider data. This includes, e.g., reducing adjacent data points that are too close to each other in depth/pressure within a yo-yo, and extracting valid individual glider yo-yos. Note that the Morison method can be conveniently applied to the entire time series of glider mission at one time, whereas the Garau method can only be applied to one glider yo-yo at a time. In the Garau method, the correction parameters, estimated from a glider yo-yo, may vary for different yo-yos; (2) For each yo-yo containing both downcast and upcast profiles of CTD data, apply the Garau method in conjunction with the median filter; (3) Concatenate the time series of individual yo-yos to form a long time series for a glider mission or transect; and (4) Further average between the downcast and upcast salinity profiles to get a single vertical profile for each glider yo-yo, depending on the applications of the glider data.

Some glider manufacturers may have already switched for pumped CTDs, which could improve the quality of salinity calculations.^{43,63} However, unpumped CTDs are still widely used in oceanographic observations. Our proposed method may help to better quality control the archived and real-time glider salinity data, as sharp thermoclines may widely exist in the world's oceans. The salinity correction was based on a Slocum glider data set. The proposed technique is also likely useful for other applications in which unpumped CTD measurements are made, for example, underway CTD.⁶⁴

Underwater gliders have been increasingly employed as an important component of coastal ocean observing systems. A vision of developing a sustained glider

network for the US coastal oceans can be seen in the IOOS National Underwater Glider Network Plan.^{65,66} It is critical to perform a proper quality assurance and quality control to the collected real-time data.⁶⁷ Our proposed method can be implemented as an additional improvement to this process before the real-time data are provided to users for decision-making.⁶⁸

ACKNOWLEDGMENTS

Support was by ONR Grant #N00014-10-1-0785, NOAA grant #'s NA06NOS4780246 and NA07NOS4730409 (the first being for the ECOHAB program and the second being through the NOAA IOOS Office for the SECOORA program), NSF grant # OCE-0741705, NASA Ocean Surface Topography Science Team (OSTST) grant # NNX13AE18G, and the Gulf of Mexico Research Institute through the Florida State University Deep-C Program. A University of South Florida (USF) College of Marine Science (CMS) internal award also helped facilitate this work. The CMS-USF glider group staff were responsible for the maintenance and deployment of the gliders as well as preliminary data processing. Dr. Carol Janzen at Sea-Bird Electronics provided enlightening discussions on the glider data acquisition system and the CTD sensors. This is CPR Contribution 37.

REFERENCES

1. Rudnick D, Davis R, Eriksen C, Fratantoni D, Perry M. Underwater gliders for ocean research. *Mar Technol Soc J* 2004;38:73–84.
2. Fratantoni DM, Haddock SHD. Introduction to the autonomous ocean sampling network (AOSN) program. *Deep Sea Res Part II* 2009;56:61.
3. Robbins C, Kirkpatrick GJ, Blackwell SM, Hillier J, Knight CA, Moline MA. Improved monitoring of HABs using autonomous underwater vehicles (AUV). *Harmful Algae* 2006;5:749–61.
4. Stommel H. The SLOCUM mission. *Oceanography* 1989;19:22–5.
5. Webb DC, Simonetti PJ, Jones CP. SLOCUM: an underwater glider propelled by environmental energy. *IEEE J Ocean Eng* 2001;26:447–52.
6. Eriksen CC, Osse TJ, Light RD, Wen T, Lehman TW, Sabin PL, et al. Seaglider: a long-range autonomous underwater vehicle for oceanographic research. *IEEE J Ocean Eng* 2001;26:424–36.
7. Sherman J, Davis RE, Owens WB, Valdes J. The autonomous underwater glider “Spray”. *IEEE J Ocean Eng* 2001;26(4):437–46.
8. Davis RE, Ohman MD, Rudnick DL, Sherman JT, Hodges B. Glider surveillance of physics and biology in the southern California current system. *Limnol Oceanogr* 2008; 53:2151–68.
9. Pierce SD, Barth JA, Shearman RK, Erofeev AY. Declining oxygen in the northeast Pacific. *J Phys Oceanogr* 2012;42:495–501.
10. Glenn S, Jones C, Twardowski M, Bowers L, Kerfoot J, Kohut J, et al. Glider observations of sediment resuspension in a Middle Atlantic bight fall transition storm. *Limnol Oceanogr* 2009;53:2180–96.

11. Schofield O, Kohut J, Glenn S, Morell J, Capella J, Corredor J, et al. A regional slocum glider network in the Mid-Atlantic bight leverages broad community engagement. *Mar Technol Soc J* 2010;44:185–95.
12. Zhao J, Hu C, Lenes JM, Weisberg RH, Lembke C, English D, et al. Three-dimensional structure of a Karenia brevis bloom: observations from gliders, satellites, and field measurements. *Harmful Algae* 2013;29:22–30. <http://dx.doi.org/10.1016/j.hal.2013.07.004>.
13. Weisberg RH, Zheng L, Liu Y, Murawski S, Hu C, Paul J. Did Deepwater horizon hydrocarbons transit to the west Florida continental shelf? *Deep Sea Res Part II* 2014. <http://dx.doi.org/10.1016/j.dsr2.2014.02.002>.
14. Weisberg RH, Zheng L, Liu Y, Lembke C, Lenes JM, Walsh JJ. Why a red tide was not observed on the west Florida continental shelf in 2010. *Harmful Algae* 2014;38:119–26. <http://dx.doi.org/10.1016/j.hal.2014.04.010>.
15. Pan C, Zheng L, Weisberg RH, Liu Y, Lembke C. Comparisons of different ensemble schemes for glider data assimilation on West Florida shelf. *Ocean Model* 2014;81:13–24. <http://dx.doi.org/10.1016/j.ocemod.2014.06.005>.
16. Perry RL, DiMarco SF, Walpert J, Guinasso Jr NL, Knap A. *Glider operations in the northwestern Gulf of Mexico*. San Diego: MTS/IEEE Oceans 2013; 2013. www.mtsjournal.org/Papers/PDFs/130503-198.pdf.
17. Ruiz S, Pascual A, Garau B, Faugere Y, Alvarez A, Tintoré J. Mesoscale dynamics of the Balearic Front, integrating glider, ship and satellite data. *J Mar Syst* 2009;78:S3–16. <http://dx.doi.org/10.1016/j.jmarsys.2009.01.007>.
18. Baird ME, Suthers IM, Griffin DA, Hollings B, Pattiaratchi C, Everett JD, et al. The effect of surface flooding on the physical–biogeochemical dynamics of a warm-core eddy off southeast Australia. *Deep Sea Res Part II* 2011;58:592–605. <http://dx.doi.org/10.1016/j.dsr2.2010.10.002>.
19. Pattiaratchi C, Hollings B, Woo M, Welhena T. Dense shelf water formation along the south-west Australian inner shelf. *Geophys Res Lett* 2011;38:L10609. <http://dx.doi.org/10.1029/2011GL046816>.
20. Roughan M, Schaeffer A, Suthers I. *Sustained ocean observing along the coast of south-eastern Australia: NSW-IMOS 2007–2014*. 2015 [Chapter 6 of this book].
21. Gregg MC, Hess WC. Dynamic response calibration of sea-bird temperature and conductivity probes. *J Atmos Ocean Technol* 1985;2:304–13.
22. Lueck RG. Thermal inertia of conductivity cells: theory. *J Atmos Ocean Technol* 1990;7:741–55.
23. Lueck RG, Picklo JJ. Thermal inertia of conductivity cells: observations with a sea-bird cell. *J Atmos Ocean Technol* 1990;7:756–68.
24. Morison J, Andersen R, Larson N, D’Asaro E, Boyd T. The correction for thermal-lag effects in sea-bird CTD data. *J Atmos Ocean Technol* 1994;11:1151–64.
25. Johnson GC, Toole JM, Larson NG. Sensor corrections for sea-bird SBE-41CP and SBE-41 CTDs. *J Atmos Ocean Technol* 2007;24:1117–11301.
26. Mensah V, Le Menn M, Morel Y. Thermal mass correction for the evaluation of salinity. *J Atmos Ocean Technol* 2009;26:665–72.
27. Bishop CM. *Sensor Dynamics of autonomous underwater gliders* [Masters thesis], Memorial University of Newfoundland; 2008.
28. Frajka-Williams E, Eriksen CC, Rhines PB, Harcourt RR. Determining vertical water velocities from seaglider. *J Atmos Ocean Technol* 2011;28:1641–56.
29. Garau B, Ruiz S, Zhang WG, Pascual A, Heslop E, Kerfoot J, et al. Thermal lag correction on slocum CTD glider data. *J Atmos Ocean Technol* 2011;28:1065–71.

30. Castelao R, Glenn S, Schofield O, Chant R, Wilkin J, Kohut J. Seasonal evolution of hydrographic fields in the central Middle Atlantic bight from glider observations. *Geophys Res Lett* 2008;35:L03617. <http://dx.doi.org/10.1029/2007GL032335>.
31. Hodges BA, Fratantoni DM. A thin layer of phytoplankton observed in the Philippine sea with a synthetic moored array of autonomous gliders. *J Geophys Res* 2009;114:C10020. <http://dx.doi.org/10.1029/2009JC005317>.
32. Chu PC, Fan CW. Optimal linear fitting for objective determination of ocean mixed layer depth from glider profiles. *J Atmos Ocean Technol* 2010;27:1893–8.
33. Shulman I, Rowley C, Anderson S, DeRada S, Kindle J, Martin P, et al. Impact of glider data assimilation on coastal model predictions. *Deep Sea Res Part II* 2009;56:188–98.
34. Zhang WG, Wilkin JL, Arango HG. Towards an integrated observation and modeling system in the New York Bight using variational methods. Part I: 4DVAR data assimilation. *Ocean Model* 2010;53(3):119–33.
35. Pan C, Yaremchuk M, Nechaev D, Ngodock H. Variational assimilation of glider data in Monterey Bay. *J Mar Res* 2011;69:331–46.
36. Troupin C, Pascual A, Valladeau G, Pujol I, Lana A, Heslop E, et al. Illustration of the emerging capabilities of SARAL/AltiKa in the coastal zone using a multi-platform approach. *Adv Space Res* 2014. <http://dx.doi.org/10.1016/j.asr.2014.09.011>.
37. Perry MJ, Sackmann BS, Eriksen CC, Lee CM. Seaglider observations of blooms and subsurface chlorophyll maxima off the Washington coast. *Limnol Oceanogr* 2008;53:2169–79.
38. Alvarez A, Mourre B. Oceanographic field estimates from remote sensing and glider fleets. *J Atmos Ocean Technol* 2012. <http://dx.doi.org/10.1175/JTECH-D-12-00015.1>.
39. Send U, Regier L, Jones B. Use of underwater gliders for acoustic data retrieval from subsurface oceanographic instrumentation and bidirectional communication in the deep ocean. *J Atmos Ocean Technol* 2013;30:984–98.
40. Eriksen CC. Salinity estimation using an un-pumped conductivity cell on an autonomous underwater glider. In: *Extended abstracts, fourth EGO conf., Larnaca, Cyprus*. EGO; 2009. p. 9.
41. Ruiz S, Renault L, Garau B, Tintoré J. Underwater glider observations and modeling of an abrupt mixing event in the upper ocean. *Geophys Res Lett* 2012;39:L01603. <http://dx.doi.org/10.1029/2011GL050078>.
42. Bouffard J, Renault L, Ruiz S, Pascual A, Dufau C, Tintoré J. Sub-surface small scale eddy dynamics from multi-sensor observations and modeling. *Prog Oceanogr* 2012. <http://dx.doi.org/10.1016/j.pocean.2012.06.007>.
43. Janzen CD, Creed EL. Physical oceanographic data from seaglider trials in stratified coastal waters using a new pumped payload CTD. In: *Proceedings of oceans 2011 MTS/IEEE, Kona, Hawaii, USA, September 19–23, 2011*, ISBN 978-1-4577-1427-6. p. 1–7.
44. Pinot J-M, Velez P, Tintore J, Lopez-Jurado JL. The thermal-lag effect in SBE-25 CTDs: importance of correcting data collected in the Mediterranean summer thermocline. *Sci Mar* 1997;61:221–5.
45. Weisberg RH, He R, Liu Y, Virmani JI. West Florida shelf circulation on synoptic, seasonal, and inter-annual time scales. In: Sturges W, Lugo-Fernandez A, editors. *Circulation in the Gulf of Mexico: observations and models*, vol. 161. Washington, D.C: AGU; 2005. p. 325–47.

46. Weisberg RH, Liu Y, Mayer DA. West Florida shelf mean circulation observed with long-term moorings. *Geophys Res Letts* 2009;36:L19610. <http://dx.doi.org/10.1029/2009GL040028>.
47. Liu Y, Weisberg RH, Merz CR, Lichtenwalner S, Kirkpatrick GJ. HF radar performance in a low-energy environment: CODAR seasonde experience on the West Florida Shelf. *J Atmos Ocean Technol* 2010;27:1689–710. <http://dx.doi.org/10.1175/JTECHO720.1>.
48. Merz CR, Weisberg RH, Liu Y. Evolution of the USF/CMS CODAR and WERA HF radar network. *Proc. MTS/IEEE Oceans* 2012;12:1–5. <http://dx.doi.org/10.1109/OCEANS.2012.6404947>.
49. Liu Y, Weisberg RH, Hu C, Kovach C, Riethmüller R. Evolution of the loop current system during the deepwater horizon oil spill event as observed with drifters and satellites. In: Liu Y, et al., editors. *Monitoring and modeling the deepwater horizon oil spill: a record-breaking enterprise*. *Geophys. Monogr. Ser.*, vol. 195. Washington, D.C: AGU; 2011. p. 91–101. <http://dx.doi.org/10.1029/2011GM001127>.
50. Weisberg RH, Liu Y, Merz CR, Virmani JI, Zheng L. A critique of alternative power generation for Florida by mechanical and solar means. *Mar Technol Soc J* 2012;46(5):12–23. <http://dx.doi.org/10.4031/MTSJ.46.5.1>.
51. Liu Y, Weisberg RH. Ocean currents and sea surface heights estimated across the West Florida shelf. *J Phys Oceanogr* 2007;37(6):1697–713. <http://dx.doi.org/10.1175/JPO3083.1>.
52. Virmani JI, Weisberg RH. Features of the observed annual ocean-atmosphere flux variability on the West Florida Shelf. *J Clim* 2003;16:734–45.
53. He R, Weisberg RH. West Florida shelf circulation and temperature budget for the 1999 spring transition. *Cont Shelf Res* 2002;22:719–48.
54. He R, Weisberg RH. West Florida shelf circulation and temperature budget for the 1998 fall transition. *Cont Shelf Res* 2003;23:777–800.
55. Liu Y, Weisberg RH. Seasonal variability on the West Florida shelf. *Prog Oceanogr* 2012;104:80–98. <http://dx.doi.org/10.1016/j.pocean.2012.06.001>.
56. Weisberg RH, He R. Local and deep-ocean forcing contributions to anomalous water properties on the West Florida shelf. *J Geophys Res* 2003;108(C6):3184. <http://dx.doi.org/10.1029/2002JC001407>.
57. Hopkins J, Sharples J, Huthnance JM. On-shelf transport of slope water lenses within the seasonal pycnocline. *Geophys Res Lett* 2012;39:L08604. <http://dx.doi.org/10.1029/2012GL051388>.
58. Bouffard J, Pascual A, Ruiz S, Faugère Y, Tintoré J. Coastal and mesoscale dynamics characterization using altimetry and gliders: a case study in the Balearic sea. *J Geophys Res* 2010;115:C10029. <http://dx.doi.org/10.1029/2009JC006087>.
59. Bray NA. Salinity calculation techniques for separately digitized fast response and platinum resistance CTD temperature sensors. *Deep Sea Res* 1987;34:627–32.
60. Emery WJ, Thomson RE. *Data analysis methods in physical oceanography*. 2nd Rev ed. Elsevier; 2001. 658p.
61. Pascual A, Ruiz S, Tintoré J. Combining new and conventional sensors to study the Balearic current. *Sea Technol* 2010;51:32–6.
62. Helber RW, Kara AB, Richman JG, Carnes MR, Barron CN, Hurlburt HE, et al. Temperature versus salinity gradients below the ocean mixed layer. *J Geophys Res* 2012;117:C05006. <http://dx.doi.org/10.1029/2011JC007382>.

3. Alvarez A, Stoner R, Maguer A. *Performance of pumped and un-pumped CTDs in an underwater glider*. San Diego, CA: IEEE Oceans 2013; 2013.
4. Ullman DS, Herbert D. Processing of underway CTD data. *J Atmos Ocean Technol* 2014; **31**:984–98. <http://dx.doi.org/10.1175/JTECH-D-13-00200.1>.
5. U.S. IOOS. *National underwater glider network Plan*. 2014. http://www.ioos.noaa.gov/glider/strategy/natl_glider_ntwrk_plan_draft_v9.pdf.
6. Willis S. *National observing systems in a global context*. 2015 [Chapter 2 of this book].
7. U.S. IOOS. *Manual for real-time quality control of in-situ temperature and salinity data*. 2014. QARTOD, http://www.ioos.noaa.gov/qartod/temperature_salinity/qartod_temperature_salinity_manual.pdf.
8. Porter DE, Dorton J, Leonard L, Kelsey H, Ramage D, Cothran J, et al. *Integrating environmental monitoring and observing systems in support of science to inform decision making: case studies for the Southeast*. 2015 [Chapter 22 of this book].